Energies **2015**, *8*, 2701-2713; doi:10.3390/en8042701

OPEN ACCESS

energies

ISSN 1996-1073

www.mdpi.com/journal/energies

Article

Melting Behavior and Thermolysis of $NaBH_4$−$Mg(BH_4)_2$ and $NaBH_4$−$Ca(BH_4)_2$ Composites

Morten B. Ley, Elsa Roedern, Peter M. M. Thygesen and Torben R. Jensen *

Center for Materials Crystallography (CMC), Interdisciplinary Nanoscience Center (iNANO) and Department of Chemistry, University of Aarhus, Langelandsgade 140, DK-8000 Århus C, Denmark; E-Mails: morten.brix.ley@gmail.com (M.B.L.); roedern@chem.au.dk (E.R.); petermmthygesen@gmail.com (P.M.M.T.)

* Author to whom correspondence should be addressed; E-Mail: trj@chem.au.dk; Tel.: +45-89-42-38-94; Fax: +45-86-19-61-99.

Academic Editor: Hai-Wen Li

Received: 12 March 2015 / Accepted: 1 April 2015 / Published: 8 April 2015

Abstract: The physical properties and the hydrogen release of $NaBH_4$–$Mg(BH_4)_2$ and $NaBH_4$−$Ca(BH_4)_2$ composites are investigated using *in situ* synchrotron radiation powder X-ray diffraction, thermal analysis and temperature programmed photographic analysis. The composite, $x NaBH_4$–$(1 - x)Mg(BH_4)_2$, x = 0.4 to 0.5, shows melting/frothing between 205 and 220 °C. However, the sample does not become a transparent molten phase. This behavior is similar to other alkali-alkaline earth metal borohydride composites. In the $x NaBH_4$–$(1 - x)Ca(BH_4)_2$ system, eutectic melting is not observed. Interestingly, eutectic melting in metal borohydrides systems leads to partial thermolysis and hydrogen release at lower temperatures and the control of sample melting may open new routes for obtaining high-capacity hydrogen storage materials.

Keywords: metal borohydride; hydrogen storage; eutectic melting

1. Introduction

In order to create a new sustainable energy economy, the storage of renewable energy is essential, e.g., directly as electricity in a battery or indirectly as hydrogen in a solid state metal hydride [1–4]. Metal borohydrides can store considerable amounts of energy as hydrogen in the solid state, but tend to

exhibit poor thermodynamic and kinetic properties, which hamper their technological utilization [5,6]. In order to improve the properties for reversible solid-state hydrogen storage, continued research within energy storage materials science is required.

The structural flexibility observed for metal borohydrides is highlighted by magnesium borohydride with seven structurally different polymorphs: α-, β-, β'-, γ-, ε-, δ- and ζ-$Mg(BH_4)_2$ [7–12]. $Mg(BH_4)_2$ is among the more promising materials for hydrogen storage applications with a high gravimetric hydrogen content of 14.9 wt% H_2 and possible reformation from the decomposition products [13,14]. Calcium borohydride also exists in several structural polymorphs, α/α'-, β- and γ-$Ca(BH_4)_2$ [15,16]. $Ca(BH_4)_2$ (ρ_m = 11.56 wt% H_2) decomposes at 370 °C to CaH_2 and CaB_6, which can also be directly rehydrogenated to $Ca(BH_4)_2$ [17,18]. The finding of other bi- and tri-metallic borohydrides, like $K_2Mg(BH_4)_4$ or $LiKMg(BH_4)_5$, illustrates the structural flexibility of complex metal hydrides [19–21], which can lead to unexpected properties, such as lithium ion conductivity, as observed in, e.g., $LiCe(BH_4)_3Cl$ [22,23]. Recently, a series of 30 new complex hydride perovskite-type materials with new photophysical, electronic and hydrogen storage properties was presented [24]. Combinations of metal borohydrides and metal hydrides in reactive hydride composite systems can influence thermodynamics and tune the gas release [25–27].

Composites of alkali and alkaline earth metal borohydrides may form eutectic mixtures with a lower melting point than the two individual components or any other composition of the two metal borohydrides [28]. $0.62LiBH_4$–$0.38NaBH_4$ melts at T_m ~ 220 °C, as compared to pristine $LiBH_4$ at T_m = 280 °C and $NaBH_4$ at T_m > 500 °C, and produces a uniform clear molten phase [28,29]. $0.725LiBH_4$–$0.275KBH_4$ has the lowest eutectic melting temperature at T_m = 105 °C (KBH_4, T_m > 600 °C) [30]. The system $x$$LiBH_4$−(1 − x)$Mg(BH_4)$, x = 0.5 to 0.6, melts at T_m ~ 180 °C ($Mg(BH_4)_2$, T_m > 280 °C) and shows improved thermodynamics and kinetics, as decomposition proceeds immediately after melting and releases 7 wt% H_2 already at T = 270 °C [11,31]. $0.68LiBH_4$–$0.32Ca(BH_4)_2$ has a eutectic melting temperature at T_m = 200 °C ($Ca(BH_4)_2$, T_m = 370 °C), releases ~10 wt% H_2 at T < 400 °C and also shows partial reversibility with respect to hydrogen storage [28,32,33]. Interestingly, the systems composed of only alkali metal borohydrides produce transparent molten phases at their melting point, while mixtures of alkali and alkaline earth metal borohydrides showed frothing/bubbling at the melting point without producing a transparent molten phase [28]. These observations have prompted the present investigation of two other metal borohydride composites, $NaBH_4$–$Mg(BH_4)_2$ and $NaBH_4$−$Ca(BH_4)_2$.

2. Experimental Section

2.1. Synthesis

Magnesium borohydride, γ-$Mg(BH_4)_2$, was synthesized using a previously published method [8]. Sodium borohydride, $NaBH_4$ (Sigma-Aldrich, 98%), and calcium borohydride, $Ca(BH_4)_2$ (Sigma-Aldrich, 95%), were used as received. The samples $x$$NaBH_4$−(1 − x)$Mg(BH_4)_2$, x = 0.1, 0.2, 0.3, 0.4, 0.5, 0.6, 0.7, 0.8 and 0.9, and $x$$NaBH_4$−(1 − x)$Ca(BH_4)_2$, x = 0.335, 0.375, 0.429, 0.445, 0.5 and 0.665, were prepared by manual mixing using a mortar and pestle. The $0.5NaBH_4$–$0.5Mg(BH_4)_2$, $0.665NaBH_4$−$0.335Mg(BH_4)_2$ and $0.5NaBH_4$−$0.5Ca(BH_4)_2$ samples were prepared by ball-milling

(BM) for 240 min and applying 2 min BM and 2-min pauses (120 repetitions) using a Fritsch Pulverisette 4 planetary mill under inert conditions (argon atmosphere) in 80-mL tungsten carbide containers with tungsten carbide balls (outer diameter (o.d.) 10 mm, sample to balls mass ratio 1:40, speed of main disk 200 rpm, speed of planetary disks 560 rpm). All preparation and manipulation of the samples were performed in a glove box with a circulation purifier maintained under an argon atmosphere with less than 1 ppm of O_2 and H_2O.

2.2. In Situ Time-Resolved Synchrotron Radiation Powder X-ray Diffraction

Synchrotron radiation powder X-ray diffraction (SR-PXD) data were collected at beamline I711 at the synchrotron MAX-II in the MAX IV laboratory Lund, Sweden, with a MAR165 CCD detector system, X-ray exposure time of 30 s and selected wavelengths of 0.999991 or 1.00355 Å [34,35]. The powdered sample was mounted in a sapphire (Al_2O_3) single-crystal tube (o.d. 1.09 mm, inner diameter (i.d.) 0.79 mm) in an argon-filled glove box $p(O_2, H_2O) < 1$ ppm. The temperature was controlled with a thermocouple placed in the sapphire tube 1 mm from the sample. All obtained raw images were calibrated against a standard NIST LaB_6 sample and transformed to 2D-powder patterns using the FIT2D program [36].

2.3. Thermal Analysis

All samples, including the reactants $Mg(BH_4)_2$ and $Ca(BH_4)_2$, were studied by simultaneous thermogravimetric analysis (TGA) and differential scanning calorimetry (DSC) using a PerkinElmer STA 6000 apparatus. Additionally, the xNaBH$_4$–$(1 - x)$Mg(BH$_4$)$_2$ samples were studied by mass spectrometry (MS) using a Hiden Analytical HPR-20 QMS sampling system. The samples (approximately 3 mg) were placed in an Al crucible and heated (5 °C/min) in an argon flow of 20 mL/min. The samples exhibit vigorous frothing above 400 °C, preventing further heating of the samples during the thermal analysis experiment.

2.4. Temperature Programmed Photographic Analysis

Temperature programmed photographic analysis (TPPA) was performed using a previously described setup [28]. Photographs were collected using a digital camera whilst heating the samples from RT to 400 °C ($\Delta T/\Delta t$ = 5 °C/min). The samples (approximately 15 mg) were sealed under argon in a glass vial connected to an argon-filled balloon to maintain an inert atmosphere. A thermocouple was in contact with the sample within the glass vial to monitor the temperature during thermolysis. The glass vial was encased within an aluminum block with open viewing windows for photography, to provide near-uniform heating by rod heaters, interfaced with a temperature controller.

3. Results

3.1. Differential Scanning Calorimetry

Analysis of the melting in the samples is performed using DSC and TPPA from room temperature (RT) to 400 °C. The DSC data of the as-synthesized $Mg(BH_4)_2$ (x = 0) reveal a single event with an

onset temperature of 197 °C; see Figure 1. $NaBH_4$ is not affected by thermodynamic events below 400 °C [37]. The DSC data of the $x NaBH_4$–$(1 - x)Mg(BH_4)_2$ composites reveal two endothermic peaks with varying intensity and onset temperatures of 178 and 205 °C; see Figures 1 and S1. The first event at 178 °C is most noticeably observed in the samples of $x NaBH_4$–$(1 - x)Mg(BH_4)_2$, x = 0.1 to 0.6; see Figures 1 and S2. The second event at 205 °C is observed mainly in $x NaBH_4$–$(1 - x)Mg(BH_4)_2$, x = 0.3–0.6.

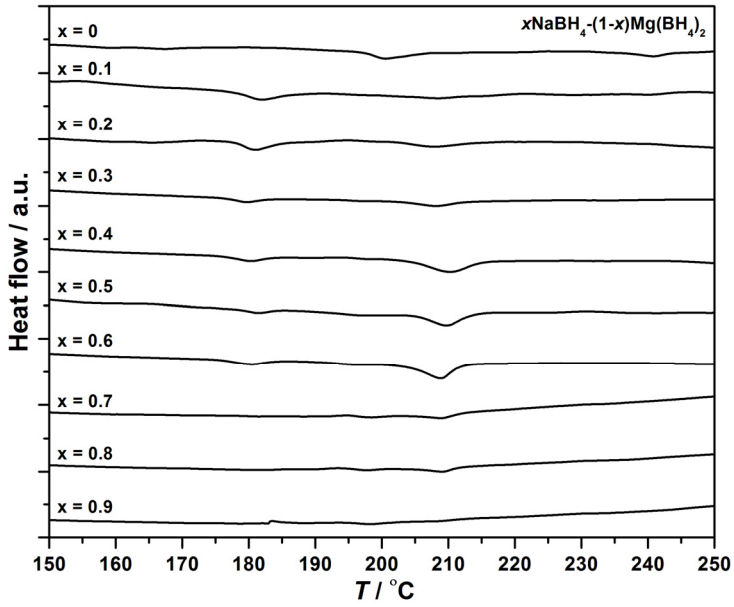

Figure 1. Normalized DSC curves of $Mg(BH_4)_2$ (x = 0) and $x NaBH_4$–$(1 - x)Mg(BH_4)_2$, x = 0.1 to 0.9, in the temperature range of 150 to 250 °C, $\Delta T/\Delta t$ = 5 °C/min.

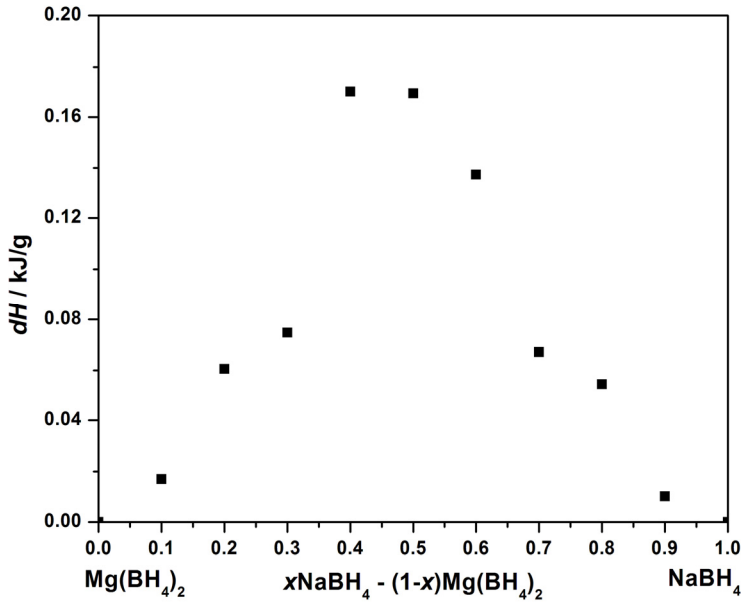

Figure 2. Integrated DSC signal in the temperature range 203 to 214 °C of the endothermic event per sample mass for $x NaBH_4$–$(1 - x)Mg(BH_4)_2$, x = 0 to 1.

The integrated area of the DSC peaks is proportional to the enthalpy change of the thermal events. The heat of reaction (dH) for the different sample compositions is extracted for the thermal events at

178 and 205 °C and shown in Figures S2 and 2, respectively. The integrated area of the peak at 205 °C is largest for the samples $0.4NaBH_4–0.6Mg(BH_4)_2$ and $0.5NaBH_4–0.5Mg(BH_4)_2$.

The DSC data from the $xNaBH_4–(1 - x)Ca(BH_4)_2$ composites are shown in the Supplementary Materials; see Figure S3. The DSC data for $Ca(BH_4)_2$ ($x = 0$) reveal an event at 345 °C. The other samples, $xNaBH_4–(1 - x)Ca(BH_4)_2$, $x = 0.335$, 0.375, 0.429, 0.429, 0.445 and 0.5, all have an endothermic peak at 280 °C followed by multiple thermal events above ~350 °C, which coincides with the single event observed for $Ca(BH_4)_2$. Furthermore, in $0.665NaBH_4–0.335Ca(BH_4)_2$, there are several small endothermic events above ~350 °C.

3.2. Temperature Programmed Photographic Analysis

In the samples $0.1NaBH_4–0.9Mg(BH_4)_2$ and $0.2NaBH_4–0.8Mg(BH_4)_2$, frothing/bubbling is observed above 280 °C; see Figure 3. In $0.4NaBH_4–0.6Mg(BH_4)_2$, $0.5NaBH_4–0.5Mg(BH_4)_2$ (BM) and $0.6NaBH_4–0.4Mg(BH_4)_2$, a decrease in the volume of the powder followed by melting/frothing are observed between 200 and 220 °C. Melting/frothing becomes more visible above 240 °C. The samples, $x = 0.8–0.9$, do not show visible changes below 400 °C, since these samples contain a majority of $NaBH_4$ with higher thermal stability. TPPA was conducted for two samples of $0.5NaBH_4–0.5Mg(BH_4)_2$ produced by ball milling and hand mixing, and the samples were found to behave similarly.

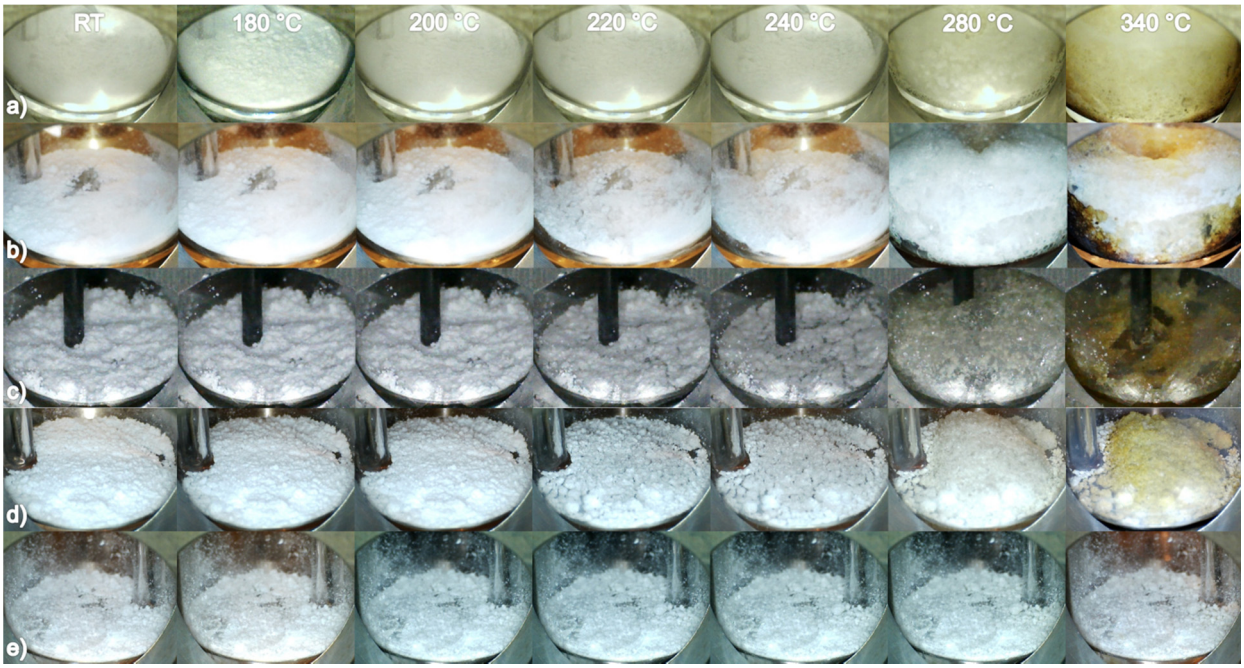

Figure 3. Temperature programmed photographic analysis (TPPA) sequence for (**a**) $0.2NaBH_4–0.8Mg(BH_4)_2$; (**b**) $0.4NaBH_4–0.6Mg(BH_4)_2$; (**c**) $0.5NaBH_4–0.5Mg(BH_4)_2$ (BM) and (**d**) $0.6NaBH_4–0.4Mg(BH_4)_2$, $0.8NaBH_4–0.2Mg(BH_4)_2$ at six selected temperatures between RT and 340 °C, $\Delta T/\Delta t = 5$ °C/min, Ar atmosphere.

The TPPA sequence for $0.5NaBH_4–0.5Ca(BH_4)_2$ is shown in Figure S4. A color change from white to light brown occurs in the sample above 290 °C. A similar behavior was observed for pure $Ca(BH_4)_2$ [28]. At 350 °C, the sample becomes partly molten. However, this also occurs for $Ca(BH_4)_2$ during thermolysis, and consequently, this is not interpreted as eutectic melting [28].

3.3. Thermogravimetric and Mass Spectrometry Analysis

The composites of $NaBH_4$ and $Mg(BH_4)_2$ are all destabilized and release hydrogen at lower temperatures as compared to $Mg(BH_4)_2$. The largest effect is observed for samples with x = 0.4–0.6; see Figure 4. In the samples with a majority of $NaBH_4$, x = 0.8–0.9, the amount of released hydrogen until 400 °C is minor, since $NaBH_4$ decomposes above 500 °C. The MS data show significant changes in the hydrogen release profile of the composites compared to $Mg(BH_4)_2$, in particular at T < 300 °C. The MS data for $x$$NaBH_4$–(1 − x)$Mg(BH_4)_2$, x = 0.4 and 0.6, show two hydrogen release reactions beginning at ~180 and 230 °C, which are not observed for $Mg(BH_4)_2$, where only a slight increase in the hydrogen signal is observed at 200 °C.

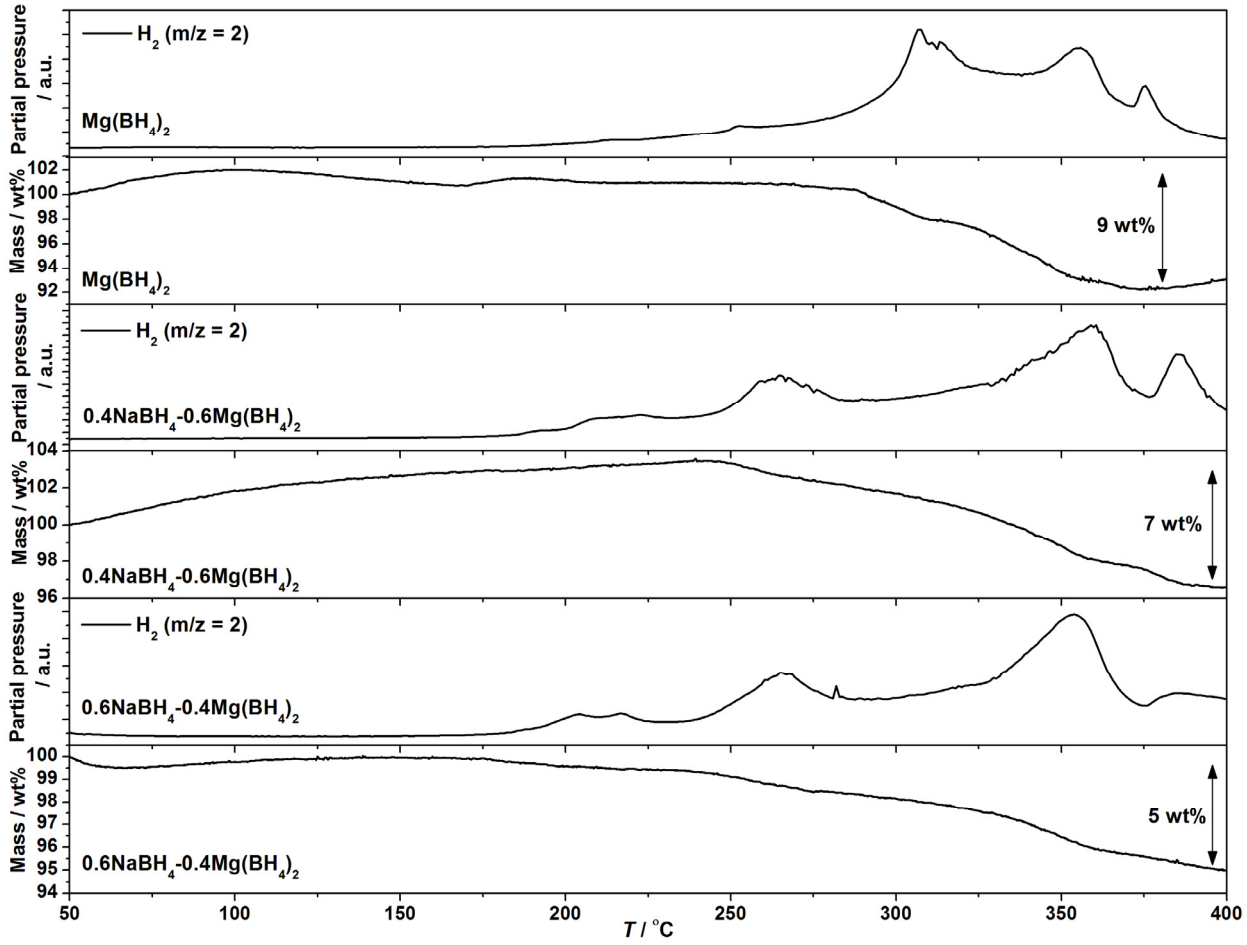

Figure 4. TGA and MS data for $Mg(BH_4)_2$, 0.4$NaBH_4$–0.6$Mg(BH_4)_2$ and 0.6$NaBH_4$–0.4$Mg(BH_4)_2$ from RT to 400 °C, $\Delta T/\Delta t$ = 5 °C/min.

The TGA registers a beginning mass loss at T ~ 240 °C for the composites and T ~ 280 °C for $Mg(BH_4)_2$. A total mass loss of 9 wt% is recorded by TGA for $Mg(BH_4)_2$ below 380 °C, which suggest partial thermolysis, $\rho_m(Mg(BH_4)_2)$ = 14.9 wt% H_2. Mass losses of 7 and 5 wt% are observed for 0.4$NaBH_4$–0.6$Mg(BH_4)_2$ and 0.6$NaBH_4$–0.4$Mg(BH_4)_2$ between 200 and 400 °C, which also suggests partial thermolysis. The theoretical hydrogen content for these samples is 14.0 and 12.7 wt% H_2.

The TGA data from the $x$$NaBH_4$–(1 − x)$Ca(BH_4)_2$ composites are shown in the Supplementary Materials; see Figure S5. The calculated hydrogen contents for the samples $Ca(BH_4)_2$,

$0.4NaBH_4–0.6Ca(BH_4)_2$ and $0.665NaBH_4–0.335Ca(BH_4)_2$, are ρ_m = 11.6, 11.3 and 11.1 wt% H_2, respectively. The mass loss from $Ca(BH_4)_2$ amounts to 6.3 wt% from 360 to 400 °C. The mass loss observed in the samples, $xNaBH_4–(1 - x)Ca(BH_4)_2$, x = 0.4 and 0.665, are 6 and 3.7 wt%, respectively. The mass loss decreases with the added amount of $NaBH_4$.

3.4. Decomposition Mechanisms Observed by in Situ SR-PXD

The *in situ* SR-PXD data for the decomposition of $0.665NaBH_4–0.335Mg(BH_4)_2$ is shown in Figure S6. Normalized diffracted intensities of selected Bragg peaks of the compounds are extracted as a function of temperature; see Figure 5. The diffraction pattern measured at RT has a broad hump in the background in the range $9 < 2\theta < 13°$, originating from amorphous $Mg(BH_4)_2$ [11,38]. The porous structure of γ-$Mg(BH_4)_2$ may have collapsed during the ball-milling, as the characteristic Bragg peaks from γ-$Mg(BH_4)_2$ are not observed at RT in the *in situ* SR-PXD experiment. Bragg peaks from $NaBH_4$ are observed at RT, indicating that $NaBH_4$ and $Mg(BH_4)_2$ do not react during ball-milling. At $T \sim 110$ °C, α-$Mg(BH_4)_2$ crystallizes, and at $T \sim 180$ °C the polymorphic phase change from the α- to β-$Mg(BH_4)_2$ occurs.

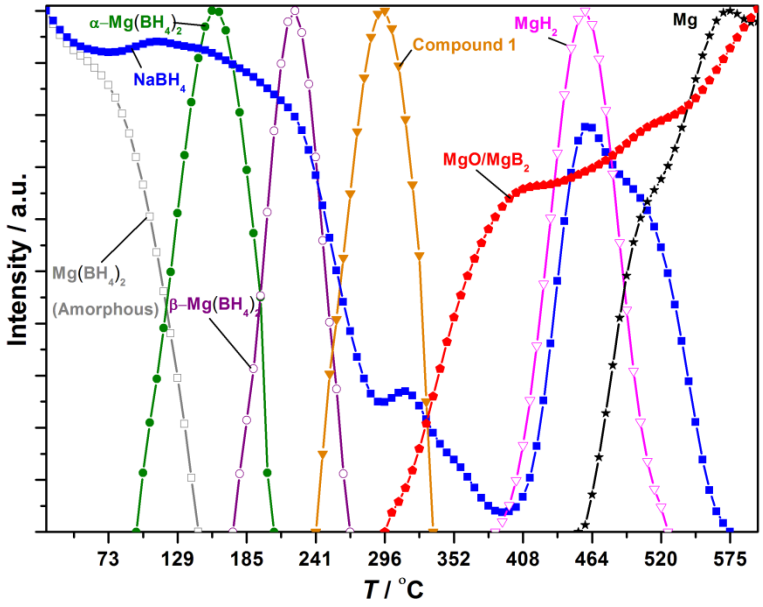

Figure 5. Normalized diffracted intensities of selected Bragg peaks from the compounds observed during the *in situ* synchrotron radiation powder X-ray diffraction (SR-PXD) experiment of $0.665NaBH_4–0.335Mg(BH_4)_2$. Legend: $NaBH_4$ (blue square), $Mg(BH_4)_2$ amorphous (grey square), α-$Mg(BH_4)_2$ (green circle), β-$Mg(BH_4)_2$ (purple circle), Compound **1** (orange triangle), MgH_2 (magenta triangle), MgO/MgB_2 (red pentagon), Mg (black star).

Crystalline β-$Mg(BH_4)_2$ disappears from the sample simultaneously with decreasing diffracted intensity from $NaBH_4$ at $T \sim 235$ °C. At $T \sim 240$ °C, an unknown compound, denoted **1**, appears, identified by three broad Bragg peaks at 2θ = 5.95°, 11.9° and 23.5°, which did not allow indexing. Compound **1** disappears at $T \sim 325$ °C simultaneous with a further decrease in intensity of Bragg peaks belonging to $NaBH_4$. At $T \sim 300$ °C, two broad peaks assigned either MgO or MgB_2 appear.

At $T \sim 400$ °C, Bragg peaks from MgH_2 are observed, and the diffracted intensity from $NaBH_4$ increases again. MgH_2 decomposes at $T \sim 465$ °C, followed by the formation of Mg metal. At $T \sim 525$ °C, the Bragg peak at $2\theta = 27.5°$ previously assigned to MgO shows a small shift to lower 2θ values, possibly due to an increased formation of MgB_2, which overlaps in peak position with MgO. At $T \sim 565$ °C, Bragg peaks from $NaBH_4$ vanish, while diffraction peaks from Mg metal, MgO and MgB_2 remain until $T = 600$ °C.

4. Discussion

4.1. Discussion of the $xNaBH_4$–$(1 - x)Mg(BH_4)_2$ Composite

Twelve samples of $NaBH_4$ and $Mg(BH_4)_2$ with varying compositions have been studied. An endothermic DSC event with an onset temperature of 178 °C was observed in all of the samples of xNaBH$_4$–$(1 - x)$Mg(BH$_4$)$_2$. This thermal event likely corresponds to the polymorphic transition of α- to β-$Mg(BH_4)_2$. Additionally, the area of the peak is larger for samples with higher $Mg(BH_4)_2$ content; see Figures 1 and S2. The polymorphic transition is also observed by *in situ* SR-PXD at 180 °C; see Figure 5. The transition temperature may be affected by the addition of $NaBH_4$, as the event occurs at a lower temperature compared to the pristine sample; see Figure 1. A similar effect is observed in the $LiBH_4$–LiCl system, where the onset temperature for the orthorhombic to hexagonal transition for $LiBH_4$ is lowered by the addition of LiCl [39].

The *in situ* SR-PXD, TPPA and DSC experiments suggest that melting occurs in the samples between 205 and 240 °C. The DSC and TPPA experiments reveal that the effect is more pronounced in the samples xNaBH$_4$–$(1 - x)$Mg(BH$_4$)$_2$, $x = 0.4$–0.6. The integrated peak area of the endothermic event with an onset temperature $T \sim 205$ °C is largest in $0.4NaBH_4$–$0.6Mg(BH_4)_2$ and $0.5NaBH_4$–$0.5Mg(BH_4)_2$, while the peak area is slightly smaller for $0.6NaBH_4$–$0.4Mg(BH_4)_2$; see Figure 2. Additionally, the TPPA experiments reveal that vigorous frothing occurs above 280 °C in samples with a majority of $Mg(BH_4)_2$, $0.2NaBH_4$–$0.8Mg(BH_4)_2$ and $0.4NaBH_4$–$0.6Mg(BH_4)_2$; see Figure 3 [11].

The *in situ* SR-PXD experiment of $0.665NaBH_4$–$0.335Mg(BH_4)_2$ shows decreasing Bragg peak intensity of $NaBH_4$ already at $T > 200$ °C. However, a major decrease in intensity only occurs at $T > 235$ °C, about 15 °C later than the frothing/melting was observed in the xNaBH$_4$–$(1 - x)$Mg(BH$_4$)$_2$, $x = 0.4$–0.6, by DSC and TPPA. This may be due to the higher amount of $NaBH_4$ [28,30].

Consequently, the xNaBH$_4$–$(1 - x)$Mg(BH$_4$)$_2$, $x = 0.4$–0.5, system is proposed to be a eutectic melting system with $T_m \sim 205$ °C. This is the first eutectic system within mixtures of alkali and alkaline metal borohydrides, which may have an excess of the alkaline earth metal borohydride. However, the melting point of $Mg(BH_4)_2$ is lower than that of $NaBH_4$ [11,28]. The lower melting metal borohydride also makes up the larger part in other eutectic metal borohydride systems [28,30]. Like in other eutectic alkali-alkaline earth metal borohydride systems, the molten phase is not a transparent liquid. This may be due to partial thermolysis and gas release of the alkaline earth metal borohydrides during melting/frothing [28].

Weak Bragg peaks assigned to Compound **1** were observed during the *in situ* SR-PXD experiment after the disappearance of β-$Mg(BH_4)_2$. Compound **1** does not show similarities to any of the recently discovered $Mg(BH_4)_2$ polymorphs [8,9,12,38]. The compound appears to crystallize from the molten

phase, possibly due to excess sodium borohydride. A minor increase in the diffracted intensity from $NaBH_4$ occurs during the decomposition of **1**, as well as the formation of MgO. Compound **1** may be analogous to compounds in the $LiBH_4$–$Ca(BH_4)_2$ system, *i.e.*, $Ca_3(BH_4)_3(BO_3)$ and $LiCa_3(BH_4)(BO_3)_2$ [40,41]. *In situ* SR-PXD shows that MgH_2 forms and decomposes at $T > 465$ °C. MgH_2 should form after the decomposition of $Mg(BH_4)_2$ at $T > 300$ °C. However, the melting/frothing in the system may make it difficult to observe Bragg peaks from MgH_2 before $T > 465$ °C.

The composites of xNaBH$_4$–$(1 - x)$Mg(BH$_4$)$_2$ are destabilized, and hydrogen release occurs at lower temperatures, as compared to $Mg(BH_4)_2$; and a larger amount of hydrogen is released in between 180 and 300 °C. However, larger amounts of $NaBH_4$ decrease the total amount of released hydrogen in the temperature range of RT to 400 °C. The MS data for hydrogen release from $0.4NaBH_4$–$0.6Mg(BH_4)_2$ and $0.6NaBH_4$–$0.4Mg(BH_4)_2$ looks very similar to $0.55LiBH_4$–$0.45Mg(BH_4)_2$ [28,31]. The decomposition mechanism might be similar for the systems, as both melt/froth and contain $Mg(BH_4)_2$. However, because of the melting/frothing in the samples, the detailed decomposition mechanism is difficult to establish by *in situ* SR-PXD. Nanoconfinement has been used to improve the kinetics of other eutectic metal borohydride systems and may also improve the xNaBH$_4$–$(1 - x)$Mg(BH$_4$)$_2$ system, whereby more hydrogen can be collected at the eutectic melting point [33,42–44]. Increased amounts of hydrogen could also be harvested by adding a catalyst [45].

4.2. Discussion of the xNaBH$_4$–(1 − x)Ca(BH$_4$)$_2$ Composite

The DSC data for each of the xNaBH$_4$–$(1 - x)$Ca(BH$_4$)$_2$, $x = 0.335$, 0.375, 0.429, 0.429, 0.445 and 0.5, samples reveal an endothermic event at ~280 °C, which may correspond to the formation of $Ca_3(BH_4)_3(BO_3)$; see Figures S3, S7 and S8. The endothermic peaks observed at ~350 °C in all of the samples of xNaBH$_4$–$(1 - x)$Ca(BH$_4$)$_2$ are assigned to the decomposition of $Ca(BH_4)_2$; see Figure S3. However, partial melting was observed by TPPA in the $0.5NaBH_4$–$0.5Ca(BH_4)_2$ sample above 350 °C; see Figure S4.

$NaBH_4$ may react with either β-$Ca(BH_4)_2$ or $Ca_3(BH_4)_3(BO_3)$ and produce Compound **2**, observed in the *in situ* SR-PXD (see Figure S7), which can explain the decreasing diffracted intensity from $NaBH_4$ above ~300 °C. Furthermore, the decomposition products from $Ca(BH_4)_2$ appear along with an increase in the diffracted intensity from $NaBH_4$. $NaBH_4$ recrystallizes after the decomposition of Compound **2**, and **2** may be analogous to $LiCa_3(BH_4)(BO_3)_2$ [41].

The mass loss observed from the samples containing $NaBH_4$ and $Ca(BH_4)_2$ remains below the theoretical content of hydrogen in all samples; see Figure S5. The hydrogen release is lower, since $NaBH_4$ only decomposes above ~500 °C. Therefore, the behavior of the composite xNaBH$_4$–$(1 - x)$Ca(BH$_4$)$_2$ during thermolysis appears to resemble that of the individual compounds with the exception of the formation of Compound **2**. Furthermore, the mixing of $NaBH_4$ and $Ca(BH_4)_2$ does not lead to destabilization and hydrogen release at a lower temperatures, as observed in the xNaBH$_4$–$(1 - x)$Mg(BH$_4$)$_2$ composite.

5. Conclusions

The composites, xNaBH$_4$–$(1 - x)$Mg(BH$_4$)$_2$ and xNaBH$_4$–$(1 - x)$Ca(BH$_4$)$_2$, were studied by *in situ* SR-PXD, temperature programmed photographic analysis and thermal analysis combined with mass

spectrometry. The composite $0.4NaBH_4$–$0.6Mg(BH_4)_2$ shows eutectic melting with $T_m \sim 205$ °C. However, the sample is not a transparent molten phase after the melting point, behaving similarly to other eutectic mixtures of alkali and alkaline earth metal borohydride mixtures. The $0.4NaBH_4$–$0.6Mg(BH_4)_2$ mixture is destabilized compared to pristine $Mg(BH_4)_2$ and releases hydrogen at a lower temperature. Only partial melting is observed for the $x NaBH_4$–$(1 - x)Ca(BH_4)_2$ composite, and it is not related to a destabilization of the system. Eutectic melting changes the decomposition mechanisms significantly. Surprisingly, the addition of a more stable metal borohydride, $NaBH_4$, to a less stable metal borohydride, $Mg(BH_4)_2$, leads to partial thermolysis and hydrogen release at lower temperatures than observed for the individual components. Indeed, the control of sample melting may open new routes for obtaining high-capacity hydrogen storage materials by tailoring the conditions for the release and uptake of hydrogen.

Supplementary Materials

Supplementary materials can be accessed at: http://www.mdpi.com/1996-1073/8/4/2701/s1.

Acknowledgments

We thank the Danish Natural Science Research Council for funding the research program DanScatt and the Danish Council for Strategic Research the project HyFillFast. We thank the MAX IV laboratory for the allocated beam time. We also thank the Center for Material Crystallography (CMC) funded by The Danish National Research Foundation for support, as well as the Carlsberg Foundation.

Author Contributions

All authors contributed to this work. Peter M. M. Thygesen and Morten Brix Ley performed the synthesis and characterization for the $x NaBH_4$–$(1 - x)Mg(BH_4)_2$ samples. Elsa Roedern and Morten Brix Ley performed the synthesis and characterization for the $x NaBH_4$–$(1 - x)Ca(BH_4)_2$ composites. Elsa Roedern and Morten Brix Ley analyzed the experimental data from all of the samples. Morten Brix Ley and Torben R. Jensen wrote the manuscript.

Conflicts of Interest

The authors declare no conflict of interest.

References

1. Ley, M.B.; Jepsen, L.H.; Lee, Y.-S.; Cho, Y.W.; Bellosta von Colbe, J.M.; Dornheim, M.; Rokni, M.; Jensen, J.O.; Sloth, M.; Filinchuk, Y.; *et al*. Complex hydrides for hydrogen storage—New perspectives. *Mater. Today* **2014**, *17*, 122–128.
2. Jepsen, L.H.; Ley, M.B.; Lee, Y.-S.; Cho, Y.W.; Dornheim, M.; Jensen, J.O.; Filinchuk, Y.; Jørgensen, J.E.; Besenbacher, F.; Jensen, T.R. Boron-nitrogen based hydrides and reactive composites for hydrogen storage. *Mater. Today* **2014**, *17*, 129–135.
3. Fichtner, M. Conversion materials for hydrogen storage and electrochemical applications—Concepts and similarities. *J. Alloys Compd.* **2011**, *509*, 529–534.

4. Goodenough, J.B.; Kim, Y. Challenges for Rechargeable Li Batteries. *Chem. Mater.* **2009**, *22*, 587–603.
5. Orimo, S.; Nakamori, Y.; Eliseo, J.R.; Züttel, A.; Jensen, C.M. Complex hydrides for hydrogen storage. *Chem. Rev.* **2007**, *107*, 4111–4132.
6. Rude, L.H.; Nielsen, T.K.; Ravnsbæk, D.B.; Bösenberg, U.; Ley, M.B.; Richter, B.; Arnbjerg, L.M.; Dornheim, M.; Filinchuk, Y.; Besenbacher, F.; *et al*. Tailoring properties of borohydrides for hydrogen storage: A review. *Phys. Status Solidi* **2011**, *208*, 1754–1773.
7. Amieiro-Fonseca, A.; Ellis, S.R.; Nuttall, C.J.; Hayden, B.E.; Guerin, S.; Purdy, G.; Soulié, J.-P.; Callear, S.K.; Culligan, S.D.; David, W.I.F.; *et al*. A multidisciplinary combinatorial approach for tuning promising hydrogen storage materials towards automotive applications. *Faraday Discuss.* **2011**, *151*, 369–384.
8. Filinchuk, Y.; Richter, B.; Jensen, T.R.; Dmitriev, V.; Chernyshov, D.; Hagemann, H. Porous and dense magnesium borohydride frameworks: Synthesis, stability, and reversible absorption of guest species. *Angew. Chem.* **2011**, *123*, 11358–11362.
9. David, W.I.F.; Callear, S.K.; Jones, M.O.; Aeberhard, P.C.; Culligan, S.D.; Pohl, A.H.; Johnson, S.R.; Ryan, K.R.; Parker, J.E.; Edwards, P.P.; *et al*. The structure, thermal properties and phase transformations of the cubic polymorph of magnesium tetrahydroborate. *Phys. Chem. Chem. Phys.* **2012**, *14*, 11800–11807.
10. Her, J.H.; Stephens, P.W.; Gao, Y.; Soloveichik, G.L.; Rijssenbeek, J.; Andrus, M.; Zhao, J.C. Structure of unsolvated magnesium borohydride $Mg(BH_4)_2$. *Acta Crystallogr. B* **2007**, *63*, 561–568.
11. Paskevicius, M.; Pitt, M.P.; Webb, C.J.; Sheppard, D.A.; Filsø, U.; Gray, E.M.; Buckley, C.E. *In-Situ* X-ray Diffraction Study of γ-$Mg(BH_4)_2$ Decomposition. *J. Phys. Chem. C* **2012**, *116*, 15231–15240.
12. Richter, B.; Ravnsbæk, D.B.; Tumanov, N.; Filinchuk, Y.; Jensen, T.R. Manganese borohydride; synthesis and characterization. *Dalt. Trans.* **2015**, *44*, 3988–3996.
13. Pistidda, C.; Garroni, S.; Dolci, F.; Bardají, E.G.; Khandelwal, A.; Nolis, P.; Dornheim, M.; Gosalawit, R.; Jensen, T.; Cerenius, Y.; *et al*. Synthesis of amorphous $Mg(BH_4)_2$ from MgB_2 and H2 at room temperature. *J. Alloys Compd.* **2010**, *508*, 212–216.
14. Severa, G.; Rönnebro, E.; Jensen, C.M. Direct hydrogenation magnesium boride to magnesium borohydride: Demonstration of >11 weight percent reversible hydrogen storage. *Chem. Commun.* **2010**, *46*, 421–423.
15. Filinchuk, Y.; Ronnebro, E.; Chandra, D. Crystal structures and phase transformations in $Ca(BH_4)_2$. *Acta Mater.* **2009**, *57*, 732–738.
16. Aeberhard, P.C.; Refson, K.; Edwards, P.P.; David, W.I.F. High-pressure crystal structure prediction of calcium borohydride using density functional theory. *Phys. Rev. B* **2011**, *83*, 174102.
17. Riktor, M.D.; Sørby, M.H.; Chłopek, K.; Fichtner, M.; Hauback, B.C. The identification of a hitherto unknown intermediate phase CaB_2H_x from decomposition of $Ca(BH_4)_2$. *J. Mater. Chem.* **2009**, *19*, 2754–2759.
18. Barkhordarian, G.; Jensen, T.R.; Doppiu, S.; Bösenberg, U.; Borgschulte, A.; Gremaud, R.; Cerenius, Y.; Dornheim, M.; Klassen, T.; Bormann, R. Formation of $Ca(BH_4)_2$ from hydrogenation of CaH_2+MgB_2 composite. *J. Phys. Chem. C* **2008**, *112*, 2743–2749.

19. Schouwink, P.; D'Anna, V.; Ley, M.B.; Lawson Daku, L.M.; Richter, B.; Jensen, T.R.; Hagemann, H.; Černý, R. Bimetallic borohydrides in the system $M(BH_4)_2$—KBH_4 (M = Mg, Mn): On the structural diversity. *J. Phys. Chem. C* **2012**, *116*, 10829–10840.
20. Schouwink, P.; Ley, M.B.; Jensen, T.R.; Smrčok, L.; Černý, R. Borohydrides: From sheet to framework topologies. *Dalton Trans.* **2014**, *43*, 7726–7733.
21. Nickels, E.A.; Jones, M.O.; David, W.I.F.; Johnson, S.R.; Lowton, R.L.; Sommariva, M.; Edwards, P.P. Tuning the Decomposition Temperature in Complex Hydrides: Synthesis of a Mixed Alkalali Metal Borohydride. *Angew. Chem. Int. Ed.* **2008**, *47*, 2817–2819.
22. Ley, M.B.; Ravnsbæk, D.B.; Filinchuk, Y.; Lee, Y.-S.; Janot, R.; Cho, Y.W.; Skibsted, J.; Jensen, T.R. $LiCe(BH_4)_3Cl$, a New Lithium-Ion Conductor and Hydrogen Storage Material with Isolated Tetranuclear Anionic Clusters. *Chem. Mater.* **2012**, *24*, 1654–1663.
23. Ley, M.B.; Boulineau, S.; Janot, R.; Filinchuk, Y.; Jensen, T.R. New li ion conductors and solid state hydrogen storage materials: $LiM(BH_4)_3Cl$, M = La, Gd. *J. Phys. Chem. C* **2012**, *116*, 21267–21276.
24. Schouwink, P.; Ley, M.B.; Tissot, A.; Hagemann, H.; Jensen, T.R.; Smrčok, L.; Černý, R. Structure and properties of complex hydride perovskite materials. *Nat. Commun.* **2014**, *5*, 5706.
25. Vajo, J.J.; Skeith, S.L.; Mertens, F. Reversible storage of hydrogen in destabilized $LiBH_4$. *J. Phys. Chem. B* **2005**, *109*, 3719–3722.
26. Dornheim, M.; Doppiu, S.; Barkhordarian, G.; Bösenberg, U.; Klassen, T.; Gutfleisch, O.; Bormann, R. Hydrogen storage in magnesium-based hydrides and hydride composites. *Scr. Mater.* **2007**, *56*, 841–846.
27. Roedern, E.; Jensen, T.R. Thermal decomposition of $Mn(BH_4)_2$−$M(BH_4)_x$ and $Mn(BH_4)_2$−MH_x composites with M = Li, Na, Mg, and Ca. *J. Phys. Chem. C* **2014**, *118*, 23567–23574.
28. Paskevicius, M.; Ley, M.B.; Sheppard, D.A.; Jensen, T.R.; Buckley, C.E. Eutectic melting in metal borohydrides. *Phys. Chem. Chem. Phys.* **2013**, *15*, 19774–19789.
29. Semenenko, K.N.; Chavgun, A.P.; Surov, V.N. Interaction of sodium tetrahydroborate with potassium and lithium tetrahydroborates. *Russ. J. Inorg. Chem.* **1971**, *16*, 271–273.
30. Ley, M.B.; Roedern, E.; Jensen, T.R. Eutectic melting of $LiBH_4$-KBH_4. *Phys. Chem. Chem. Phys.* **2014**, *16*, 24194–24199.
31. Bardaji, E.G.; Zhao-Karger, Z.; Boucharat, N.; Nale, A.; van Setten, M.J.; Lohstroh, W.; Rohm, E.; Catti, M.; Fichtner, M. $LiBH_4$-$Mg(BH_4)_2$: A physical mixture of metal borohydrides as hydrogen storage material. *J. Phys. Chem. C* **2011**, *115*, 6095–6101.
32. Lee, J.Y.; Ravnsbæk, D.; Lee, Y.-S.; Kim, Y.; Cerenius, Y.; Shim, J.-H.; Jensen, T.R.; Hur, N.H.; Cho, Y.W. Decomposition reactions and reversibility of the $LiBH_4$-$Ca(BH_4)_2$ composite. *J. Phys. Chem. C* **2009**, *113*, 15080–15086.
33. Lee, H.-S.; Lee, Y.-S.; Suh, J.-Y.; Kim, M.; Yu, J.-S.; Cho, Y.W. Enhanced Desorption and Absorption properties of eutectic $LiBH_4$-$Ca(BH_4)_2$ infiltrated into mesoporous carbon. *J. Phys. Chem. C* **2011**, *115*, 20027–20035.
34. Cerenius, Y.; Stahl, K.; Svensson, L.A.; Ursby, T.; Oskarsson, A.; Albertsson, J.; Liljas, A. The crystallography beamline I711 at MAX II. *J. Synchrotron Radiat.* **2000**, *7*, 203–208.

35. Jensen, T.R.; Nielsen, T.K.; Filinchuk, Y.; Jørgensen, J.E.; Cerenius, Y.; Gray, E.M.; Webb, C.J. Versatile *in situ* powder X-ray diffraction cells for solid–gas investigations. *J. Appl. Crystallogr.* **2010**, *43*, 1456–1463.
36. Hammersley, A.P.; Svensson, S.O.; Hanfland, M.; Fitch, A.N.; Hausermann, D. Two-dimensional detector software: From real detector to idealised image or two-theta scan. *High Press. Res.* **1996**, *14*, 235–248.
37. Martelli, P.; Caputo, R.; Remhof, A.; Mauron, P.; Borgschulte, A.; Züttel, A. Stability and decomposition of $NaBH_4$. *J. Phys. Chem. C* **2010**, *114*, 7173–7177.
38. Ban, V.; Soloninin, A.V.; Skripov, A.V.; Hadermann, J.; Abakumov, A.; Filinchuk, Y. Pressure-collapsed amorphous $Mg(BH_4)_2$: An Ultradense complex hydride showing a reversible transition to the porous framework. *J. Phys. Chem. C* **2014**, *118*, 23402–23408.
39. Arnbjerg, L.M.; Ravnsbæk, D.B.; Filinchuk, Y.; Vang, R.T.; Cerenius, Y.; Besenbacher, F.; Jørgensen, J.-E.; Jakobsen, H.J.; Jensen, T.R. Structure and dynamics for $LiBH_4$—LiCl solid solutions. *Chem. Mater.* **2009**, *21*, 5772–5782.
40. Riktor, M.D.; Filinchuk, Y.; Vajeeston, P.; Bardají, E.G.; Fichtner, M.; Fjellvåg, H.; Sørby, M.H.; Hauback, B.C. The crystal structure of the first borohydride borate, $Ca_3(BD_4)_3(BO_3)$. *J. Mater. Chem.* **2011**, *21*, 7188–7193.
41. Lee, Y.-S.; Filinchuk, Y.; Lee, H.-S.; Suh, J.-Y.; Kim, J.W.; Yu, J.-S.; Cho, Y.W. On the formation and the structure of the first bimetallic borohydride borate, $LiCa_3(BH_4)(BO_3)_2$. *J. Phys. Chem. C* **2011**, *115*, 10298–10304.
42. Zhao-Karger, Z.; Witter, R.; Bardají, E.G.; Wang, D.; Cossement, D.; Fichtner, M. Altered reaction pathways of eutectic $LiBH_4$-$Mg(BH_4)_2$ by nanoconfinement. *J. Mater. Chem. A* **2013**, *1*, 3379.
43. Javadian, P.; Jensen, T.R. Enhanced hydrogen reversibility of nanoconfined $LiBH_4$–$Mg(BH_4)_2$. *Int. J. Hydrog. Energy* **2014**, *39*, 9871–9876.
44. Javadian, P.; Sheppard, D.A.; Buckley, C.E.; Jensen, T.R. Hydrogen storage properties of nanoconfined $LiBH_4$–$Ca(BH_4)_2$. *Nano Energy* **2015**, *11*, 96–103.
45. Zavorotynska, O.; Saldan, I.; Hino, S.; Humphries, T.D.; Deledda, S.; Hauback, B.C. Hydrogen cycling in γ-$Mg(BH_4)_2$ with cobalt-based additives. *J. Mater. Chem. A* **2015**, *3*, 6592–6602.